Journal of Power Sources 196 (2011) 10591–10600

Contents lists available at SciVerse ScienceDirect

Journal of Power Sources

journal homepage: www.elsevier.com/locate/jpowsour

Rotating disk electrode study of $Cs_{2.5}H_{0.5}PW_{12}O_{40}$ as mesoporous support for Pt nanoparticles for PEM fuel cells electrodes

S. Dsoke[a,1], A. Kolary-Zurowska[a,b], A. Zurowski[a,b], P. Mignini[a], P.J. Kulesza[b,**], R. Marassi[a,*]

[a] Department of Chemistry, University of Camerino, S. Agostino 1, I-62032 Camerino, Italy
[b] Department of Chemistry, University of Warsaw, Pasteura 1, PL-02-093 Warsaw, Poland

ARTICLE INFO

Article history:
Received 1 July 2011
Received in revised form 30 August 2011
Accepted 4 September 2011
Available online 10 September 2011

Keywords:
Heteropolyacid salts
Rotating disk voltammetry
Rotating ring disk voltammetry
ORR

ABSTRACT

The catalytic activity of Pt nanoparticles supported by zeolite-type mesoporous $Cs_{2.5}H_{0.5}PW_{12}O_{40}$ solid super-acid towards oxygen reduction has been explored. Pt(IV) impregnated $Cs_{2.5}H_{0.5}PW_{12}O_{40}$ was prepared by titration of an aqueous solution of phosphotungstic acid and a known quantity of H_2PtCl_6 with a solution of cesium carbonate. The H_2PtCl_6 impregnated insoluble salt was subsequently chemically or electrochemically reduced to form supported Pt nanoparticles.

HRTEM micrographs show that the reduced composites Pt–$Cs_{2.5}H_{0.5}PW_{12}O_{40}$ (Pt–$Cs_{2.5}PW_{12}$) contains Pt nanoparticles of average dimensions 2–5 nm, embedded into the porous structure of the insoluble salt. RDE and RRDE studies and fuel cell polarization data performed using thin layer composite films of Pt–$Cs_{2.5}PW_{12}$ chemically or electrochemically reduced show that the catalyst is very stable and rather efficient for oxygen reduction (ORR). The oxygen reduction wave is shifted by 60–70 mV towards more positive potentials with respect to the one obtained using electrodes prepared with a standard catalyst such as E-Tek 20% Pt–Vulcan. Analysis of the voltammetric curves demonstrates that the electrocatalytic activity of the composite electrodes is higher than that of the standard catalyst. This indicates that the solid state super-acid $Cs_{2.5}H_{0.5}PW_{12}O_{40}$ acts as co-catalyst by providing a proton rich environment in the vicinity of the Pt nanoparticles that enhances their catalytic activity towards oxygen reduction.

1. Introduction

Durability and cost are the most important issues that must be solved for a successful commercialization of proton exchange membrane fuel cells (PEMFC). Carbon supported Pt nanoparticles are by far the most used catalyst for oxygen reduction (ORR) and hydrogen oxidation (HOR) in PEMFC. Different problems, related to degradation of the Nafion membrane and carbon catalyst support, together with loss of catalytic activity of the Pt electro-catalyst, are currently important topics of basic and applied research world-wide [1,2]. Because of the high acidity, positive electrochemical potential and of the presence of water and oxygen in high concentration, the catalyst at the cathode side is particularly prone to degradation. Carbon oxidation at high potentials, enhanced by the presence of Pt, decreases the contact between the nanoparticles and the support that becomes increasingly hydrophobic causing a deterioration of the mass transport properties of the gas diffusion electrode (GDE). Loss of contact between the Pt nanoparticles and the carbon support also increases the mobility of the particles that might aggregate thus decreasing the electrochemical active surface area. Pt dissolution, and oxide formation at high potentials followed by re-deposition also contribute to the increase of the particle size [1–7].

In the attempt to solve or minimize these problems, current research follows different lines. Apart from optimizing the operating conditions by avoiding high potentials and humidity levels, one approach is the search of alternative matrices for supporting Pt nanoparticles. Several papers deal, for instance, with the use of TiO_2 [8–15] as support for Pt nanoparticles. Composite electrodes are formed by adding carbon to the Pt/TiO_2 in order to create a percolating path for electronic conductivity. As the Pt nanoparticles are supported on TiO_2, the direct contact of Pt with carbon is minimized and the carbon degradation is reduced. Interesting is also the use of electrodes in which Pt is supported on tungsten oxides [11,16–18]. These types of electrodes have been demonstrated to be able to promote oxygen reduction via hydrogen spillover. The highly conductive tungsten oxide bronzes are also effective in reducing formation of hydrogen peroxide.

* Corresponding author. Tel.: +39 737 402214.
** Co-corresponding author. Tel.: +48 22822020211.
E-mail addresses: roberto.marassi@unicam.it(R. Marassi), pkulesza@chem.uw.edu.pl (P.J. Kulesza).
[1] Present address: ZSW-Zentrum für Sonnenenergie und Wasserstoff-Forschung, Helmholtzstraße, D-89081 Ulm, Germany.

0378-7753/$ – see front matter © 2011 Elsevier B.V. All rights reserved.
doi:10.1016/j.jpowsour.2011.09.010

Heteropolyacids in fuel cell research have been the subject of several papers especially because of their ability to strongly adsorb on metal or carbon electrodes and of their high acidic character. Several research groups have explored the ability of different types of heteropolyacids to modify unsupported or carbon supported Pt nanoparticles for oxygen reduction [19–24], methanol oxidation [25–32] or as additive in membranes [33–42].

In recent papers we have been concerned with the optimization of Pt-based electrocatalyst for oxygen reduction (ORR) by modifying the surface of Pt nanoparticles with adsorbed Keggin type H_2PtCl_6 based on Si or P heteroatoms and addenda atoms such as W or Mo [19–23]. Adsorption of heteropolyanions (especially $H_3PW_{12}O_{40}$) on Pt causes a shift of the voltammetric peaks relative to formation of Pt-oxo (PtOH or PtO) species towards more positive potential. Because of a larger potential window over which platinum is not covered with platinum oxide, adsorption and activation of oxygen molecules during electrocatalysis is facilitated. Due to the interaction between heteropolianions and Pt surface by mainly corner oxygen, only a few percent of interfacial reactive platinum atoms are blocked to the access of oxygen molecules [23].

In spite of the fact that the heteropolyacids are strongly adsorbed, long-term operation of this type of electrodes may cause desorption leading to loss of the catalytic activity. One possible alternative to improve long term stability of the electrodes is the use of water insoluble heteropolyacid salts that may be easily prepared by partially exchanging protons of the parent acid with the large cations such as Cs^+, K^+, NH_4^+. The insoluble cesium salts of phosphotungstic $H_3PW_{12}O_{40}$ acid are of particular interest [43–49]. These salts are efficient solid acid catalyst for a variety of organic reaction. Partial substitution of protons in $H_3PW_{12}O_{40}$ by Cs^+ ions leads to formation of crystalline aggregates with peculiar changes of the surface area and surface acidity. The surface of $Cs_xH_{3-x}PW_{12}O_{40}$ is practically the same of that of the parent acid (about $5\,m^2\,g^{-1}$) up to $x=2$ and then rapidly increases with increasing x to reach values in excess of $100\,m^2\,g^{-1}$ ($135\,m^2\,g^{-1}$ for $Cs_{2.5}H_{0.5}PW_{12}O_{40}$) due to formation of a microporous/mesoporous structure [50] with interparticles voids. The surface acidity parallels the trend of the surface area: it increases with a bell-shaped behavior starting from $x=2$, reaches a maximum at $x=2.5$ and then decreases to zero for $x=3$. The high acidity together with the possibility to tailor the dimension of the pores has been largely exploited in organic chemistry for the development of shape selective catalysts. The surface protons are, in addition, highly mobile. This property, directly correlated with the hydration degree of the compound, has been explored in fuel cell research using pellets of $Cs_{2.5}H_{0.5}PW_{12}O_{40}$ as electrolyte [51] or in the development of self-humidifying Nafion or sulfonated poly(ether ether ketone) (SPEEK) based membranes [37,38,41,42].

The catalytic activity of solid acids cesium salts towards a variety of organic reactions has also been improved by doping the water insoluble salts with precious metals such as Pt or Pd to obtain a bi-functional shape selective catalyst [49,52–55]. Pt doped $Cs_{2.5}H_{0.5}PW_{12}O_{40}$ (Pt–$Cs_{2.5}PW_{12}$) has also been used as additive in SPEEK based membranes to reduce the hydrogen crossover in PEMFC. The Pt nanoparticles catalyze the hydrogen oxidation without affecting the insulating property of the membrane as the salt is an electronic insulator [41]. If one exclude the use of Pt–$Cs_{2.5}PW_{12}$ in membranes [41], to the best of our knowledge, the electrochemical characterization for oxygen reduction (ORR) (or hydrogen oxidation (HOR)) of composites electrodes using Pt nanoparticles supported on insoluble mesoporous salts of heteropolyacids under the conditions found in fuel cells has gone unreported. The basic idea behind this is similar to that exploited for TiO_2 or WO_3 with two possible additional advantages. The nanoparticles can be trapped inside the porous matrix mitigating/preventing particle aggregation. The electrodes may take advantage of the strong surface acidity of the compound and of the high proton mobility that may improve the kinetic of oxygen reduction that requires protons in addition to electrons. At the same time the high porosity of the salts should not affect the transport properties of the catalytic layer. As was the case of Pt nanoparticles supported on TiO_2, because of the insulating characteristic of the insoluble salts, the composite must necessarily contain a carbon additive to create a percolating electron-conducting network in the electrode. Recent patents applications deal with the description of the use of several Pt doped heteropolyacid salts in fuel cell research [56,57]. Activation of carbon-supported Pt nanoparticles by mixing with Cs salts of polyoxometallates of molybdenum and tungsten towards oxidation of methanol and ethanol has also been recently reported [58]. The same approach has also been used to enhance the ORR catalytic ac activity of carbon supported Pt–Co alloys [59]. A short report in which Pt doped $Cs_{2.5}PW_{12}$ was electrochemically prepared using a sacrificial Pt anode and used as ORR catalyst has also been published [60]. This paper deals with a study of chemically prepared Pt–$Cs_{2.5}PW_{12}$ composite electrodes with special concern to ORR using mainly RDE and RRDE voltammetry. Preliminary fuel cell data are also presented.

2. Experimental

2.1. Materials

All the chemicals were of analytical grade purity and were used without further purification. Phosphotungstic, perchloric and sulfuric acids, as well as chloroplanic acid, were obtained from Sigma Aldrich. Solutions were prepared using doubly distilled and subsequently de-ionized (Millipore Milli-Q) water. The carbon supported platinum catalyst (20% Pt/Vulcan XC-72), Vulcan-XC-72 and GDE (gas diffusion electrode) Pt loading $0.5\,mg\,cm^{-2}$ were from E-Tek. Nafion (5% alcoholic solution) and Nafion 212 membrane were obtained from Ion-Power, Inc.

2.2. Catalyst preparation

$Cs_{2.5}H_{0.5}PW_{12}O_{40}$ ($Cs_{2.5}PW_{12}$) was prepared [45] using the following steps. An aqueous solution of Cs_2CO_3 was added drop-wise to an $H_3PW_{12}O_{40}$ solution under vigorous stirring. The fine suspension was held at room temperature overnight and subsequently evaporated to dryness at 323 K. The ratio polyacid–cesium carbonate was regulated in such a way that the final stoichiometry corresponded to $Cs_{2.5}H_{0.5}PW_{12}O_{40}$. ICP-MS measurements on the dried solid gave a ratio Cs to W equal to 2.5 ± 0.05.

Pt(IV) containing solids were prepared in the same way starting from the heteropolyacid solution containing H_2PtCl_6 in different quantities depending on the desired final Pt metal content. The absence of any washing step assures that all the platinum present in the initial solution remains in the dried powder either adsorbed or trapped inside the pores of the insoluble salt. The product color is pale yellow reflecting the color of chloroplatinic acid. The prepared sample will be indicated in the following as Pt(x%)–$Cs_{2.5}PW_{12}$ with x indicating the final metal Pt loading in the salt.

Two different routes were followed to reduce the Pt(IV) to Pt: the dried solid was reduced using a 5% H_2/Argon stream at 300 °C or the Pt(IV) impregnated salt was used as such to prepare inks that were activated in situ by electrochemical means. Details on the latter procedure will be given in Section 3.

Electrodes for fuel cell experiment were prepared by brushing inks, having the same composition used for the film electrodes, containing either reduced or unreduced composites on Teflon treated Toray Carbon Paper (EC-TP1-060T) in the desired amounts. The MEA, were prepared by hot pressing (50 bar) the electrodes

(5 cm^2 active area) at 130 °C for 3 min onto a pre-treated Nafion 212 membrane.

2.3. Physical and electrochemical characterization

X-ray spectroscopy and HRTEM were used to characterize the products. X-ray has been recorded using Philips Bragg-Brentano diffractometer equipped with diffracted beam graphite monochromator. HRTEM micrographs have been obtained at the Institut de Minéralogie et de Physique des Milieux Condensés, UMPC, Paris, France using a JEOL JEM-2100F.

2.4. Electrode preparation and electrochemical measurements

Catalyst inks were prepared by ultrasonically dispersing either Pt(IV)–$Cs_{2.5}PW_{12}$ or Pt–$Cs_{2.5}PW_{12}$ (the chemically reduced product), Vulcan XC-72 and Nafion (mass ratio 1.3:1:0.07) in isopropanol. The slurry was homogenized overnight. Drops (4–5 μl) of the slurry were deposited on the GC disk of a ring disk electrode (GC disk 0.164 cm^2, Pt ring, collection efficiency 0.206) and dried for 30 min at room temperature. The electrode was polished on a cloth with a water suspension of Al_2O_3 (particle size 0.3–0.05 μm) before formation of the layer. Details on the reduction of Pt(IV) to Pt in the case of use of Pt(IV)–$Cs_{2.5}PW_{12}$ will be given in Section 3. Typically the film thickness was about 0.1 μm with a Pt metal loading of the order of 10–40 μg cm^{-2}. For comparison, heteropolyacid salt-free inks of 20% Pt/Vulcan XC-72 and Nafion were also prepared.

All the measurements were performed in 0.1 M $HClO_4$ (or 0.5 M H_2SO_4) solutions saturated with high purity oxygen, hydrogen or purged with argon using a three-compartment electrochemical cell equipped with a water jacket for temperature control (25 ± 0.5 °C). A platinum flag and a saturated Hg/Hg_2SO_4 electrode were used as counter and reference electrodes, respectively. The reference was placed in a separated compartment connected to the main cell body through a Luggin capillary. A bi-potentiostat (CH Instrument 832 workstation) was used in all experiments. The electrode was driven by a Pine rotator 636 ring-disk electrode system (Pine Instruments, USA).

A FC-05-02 5 cm^2 cell from Electrochem. Inc. controlled by a Scribner Associated 890CL fuel cell test system was used for the fuel cell experiments.

All potentials in the paper are referred to the reversible hydrogen electrode (RHE) scale. To prevent errors due to the variability of the reference electrode [61], its potential was calibrated using a Pt electrode in the same solution saturated with hydrogen at the beginning and at the end of each experiment.

3. Results and discussion

3.1. Physicochemical characterization

Fig. 1a–d shows the X-ray spectra of the acid, the $Cs_{2.5}H_{0.5}PW_{12}O_{40}$, chemically reduced Pt(5%)–$Cs_{2.5}PW_{12}$ and Pt(20%)–$Cs_{2.5}PW_{12}$, respectively. The spectra of the Pt containing salts refer to samples reduced with hydrogen at 300 °C. Given the peculiar mechanism of formation of $Cs_{2.5}PW_{12}$ during its preparation by precipitation from aqueous solution of the acid and Cs_2CO_3, the precipitates consist of ultrafine crystallites of $Cs_3PW_{12}O_{40}$ with the acid form, $H_3PW_{12}O_{40}$, epitaxially deposited on the surface. Thermal treatment at 300 °C causes migration of H^+ and Cs^+ in the solid leading to a nearly uniform solid solution in which the protons are randomly distributed through the entire bulk. However, the X-ray spectra of the as obtained dried precipitate and of the calcined products do not differ appreciably [47,48,62,63]. All the spectra present the characteristic peaks of the body centered cubic structure of the Keggin type hetero-polyacids. The X-ray spectra of the pure salts, 5% and 20% Pt–$Cs_{2.5}PW_{12}$ are essentially the same as that of the acid if one exclude the shift to higher angles caused by the contraction of cell parameters due to the substitution of the units $H_5O_2^+$ with the smaller Cs^+ ion [48]. The line broadening in the spectra of the salts is consistent with a decrease of the crystallite size in going from the acid to the salts. No clear evidences for metal Pt are found in spectrum c. This is consistent with previous results [49] and may be due to the fact that the Pt nanoparticles, embedded into the mesoporous structure, are probably too small/dispersed to give coherence in the X-ray spectra. However, the presence of Pt metal nanoparticles results from HRTEM (see below). In the case of Pt(20%)–$Cs_{2.5}PW_{12}$ the presence of the sharp peak (1 1 1) testifies the existence of metal platinum in the composite.

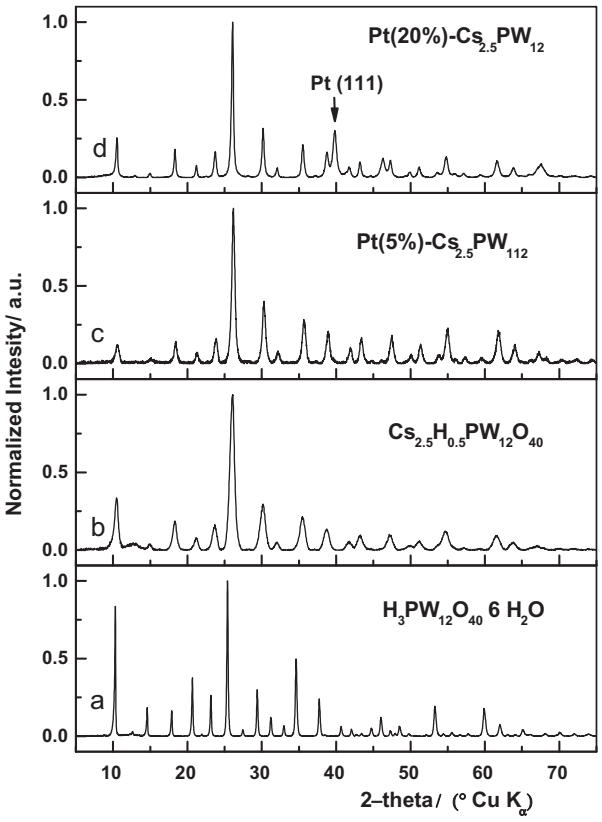

Fig. 1. X-ray spectra of $H_3PW_{12}O_{40}$ (a), $Cs_{2.5}H_{0.5}PW_{12}O_{40}$ (b), Pt(5%)–$Cs_{2.5}PW_{12}$ (c) and Pt(20%)–$Cs_{2.5}PW_{12}$.

Fig. 2a–d shows TEM micrographs of catalyst containing different amounts of Pt at different resolutions. Fig. 2 a and b refers to Pt(5%)–$Cs_{2.5}PW_{12}$ and c and d to Pt(20%)–$Cs_{2.5}PW_{12}$. The low resolution micrograph in Fig. 2a does not show any evidence of Pt nanoparticles outside the crystallites. Pt nanoparticles of average dimension in the range 2–5 nm embedded inside the pores are clearly evident in the high resolution micrograph in Fig. 2b. In the case of Pt(20%)–$Cs_{2.5}PW_{12}$ (Fig. 2c and d) Pt nanoparticles are evident both at the surface and inside the pores. On average the particles on the surface are greater (≈10–13 nm) than those embedded into the pores and this may explain the appearance of the (1 1 1) reflection in the X-ray spectra. The micrograph in Fig. 2e shows an high resolution image of a single particle isolated from a sample of electrochemically reduced Pt(5%)–$Cs_{2.5}PW_{12}$ removed from the electrode surface. The fringes of a well crystallized Pt are clearly evident. Additional data on particle size distribution in catalytic layers electrochemically reduced starting from the Pt(IV)–$Cs_{2.5}PW_{12}$ may be found in Ref. [64] that reports an in situ X-ray absorption

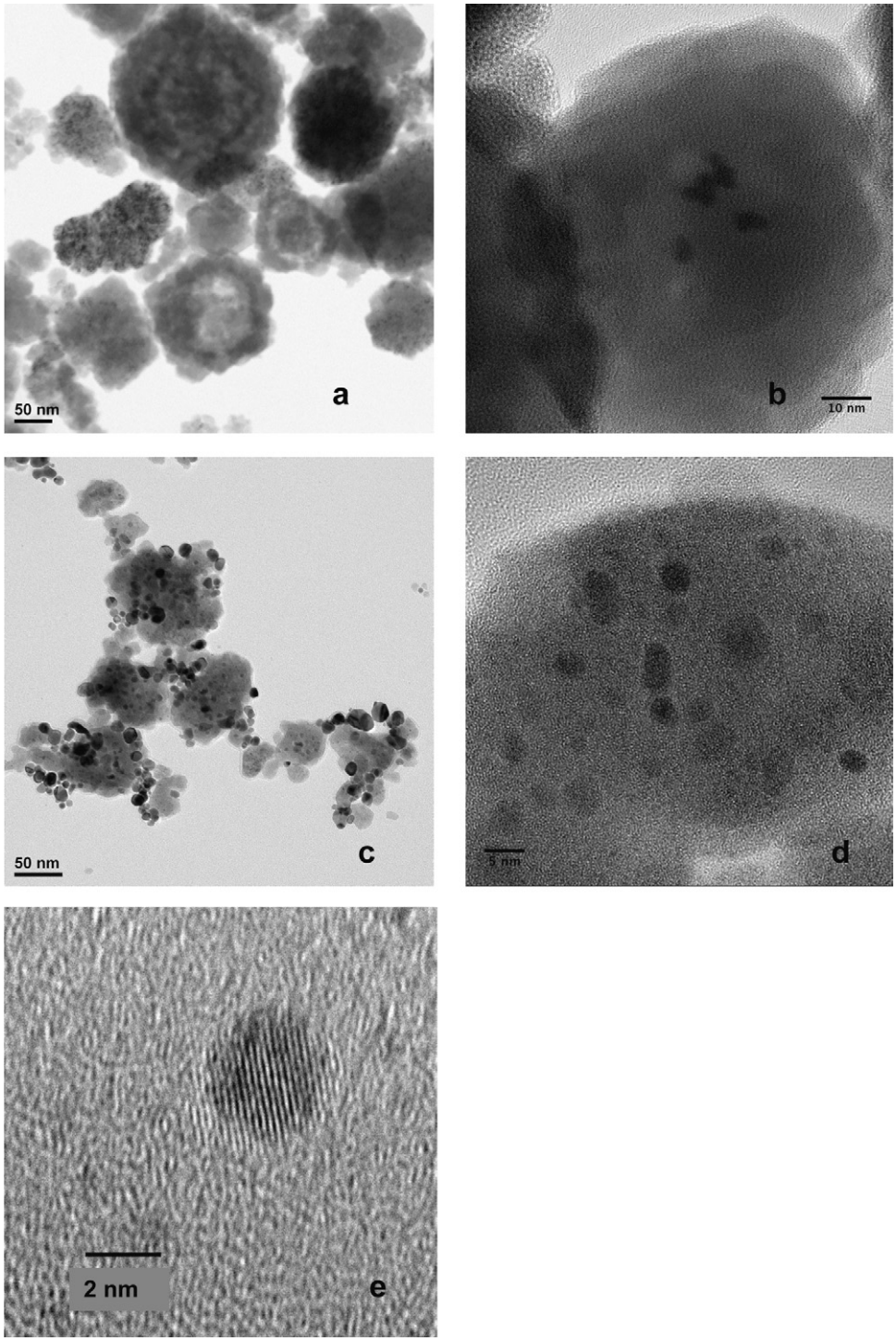

Fig. 2. HRTEM micrographs of Pt(5%)–$Cs_{2.5}PW_{12}$ (a and b) and Pt(20%)–$Cs_{2.5}PW_{12}$ (c and d); (e) single particle isolated from an electrochemically reduced electrode.

(XAS) study performed using an operating PEM fuel cell equipped with a MEA with Pt(10%)–$Cs_{2.5}PW_{12}$ electrochemically reduced as cathode catalyst. The Pt size distribution was an asymmetric Γ-like function with an average diameter equal to 2 ± 0.1 nm and a $\sigma = 0.8 \pm 0.1$.

Indirect evidences for the trapping of the Pt particles have been obtained from BET measurements. The BET surface area was found to decrease with increasing Pt content from a value of 139 $m^2\ g^{-1}$ for pure $Cs_{2.5}H_{0.5}PW_{12}O_{40}$ to about 50 and 35 $m^2\ g^{-1}$ for Pt(5%)–$Cs_{2.5}PW_{12}$ and Pt(20%)–$Cs_{2.5}PW_{12}$, respectively. This means that most of the low dimension pores (range 2–4 nm) become progressively saturated with increasing Pt content and justifies the presence of Pt nanoparticles on the surface of the salt in the case of Pt(20%)–$Cs_{2.5}PW_{12}$.

3.2. Stability test

Preliminary tests on the stability of the composites under the conditions found in PEM have been carried out by keeping a sample of Pt(20%)–$Cs_{2.5}PW_{12}$ in H_2SO_4 1 M under vigorous stirring at 70 °C for four months. Fig. 3 shows the UV–vis spectra of a 2×10^{-5} M solution of the pure acid (curve a) and of the test suspension (curve

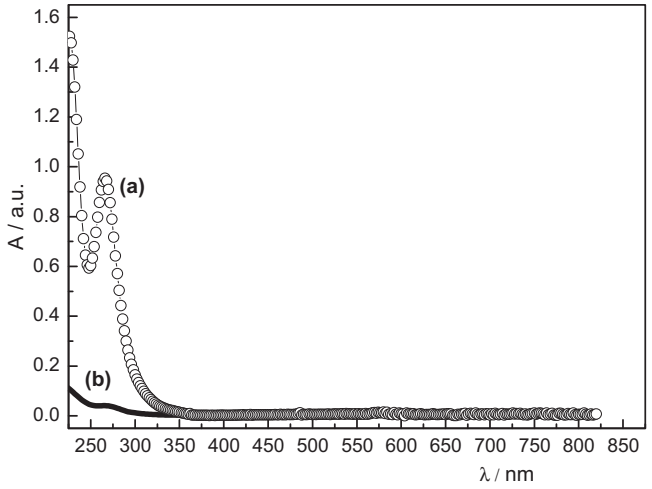

Fig. 3. UV–vis spectra of a 2.5×10^{-5} M molar solution of $H_3PW_{12}O_{40}$ in 0.5 M H_2SO_4 (◯) and of an aliquot of solution containing Pt–$Cs_{2.5}PW_{12}$ after 4 months stirring at 70 °C (- - - -). See text for details.

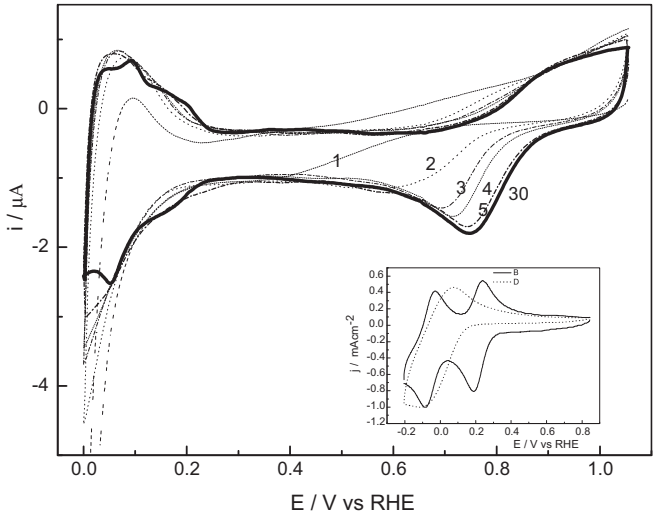

Fig. 4. Activation of a catalytic layer containing Pt(IV)–$Cs_{2.5}PW_{12}$ by cyclic voltammetry in a 0.5 M H_2SO_4 solution. Scan rate 50 mV s^{-1}. Pt loading 20 μg cm^{-2}. Insert: cyclic voltammogram at a GC electrode obtained in a 2×10^{-3} M solution of $H_3PW_{12}O_{40}$ (- - - -), scan rate 50 mV s^{-1}, and (···) with a film electrode containing Pt free $Cs_{2.5}H_{0.5}PW_{12}O_{40}$.

b). The characteristic peak at 270 nm, due to charge transfer band O–M in the spectrum of the acid, is practically absent in the case of the solution kept in contact with the salt. The small feature in the same wavelength region was present at the very beginning and did change during the experiment as demonstrated by spectra taken at regular time intervals. This means that the feature is probably related to some residual acid impurity of the salt and that no dissolution takes place during the time period of the experiment. In addition, the X-ray spectrum of the precipitate at the end of the experiment is superimposable to that of the starting material thus further demonstrating that no decomposition or changes in the structure occur upon prolonged exposure to an acidic environment at the temperature usually found in PEMFC. The stability of the support in acidic media is not surprising in view of its use as solid acid catalyst in organic reaction and has been further confirmed when, in preparing the samples for ICP analysis, the salt had to be dissolved in basic solution as acid digestion was completely ineffective.

3.3. Preparation of catalytic layer by electrochemical activation

As explained in the experimental section, the catalytic layers may be prepared either by mixing the reduced composite with Vulcan and Nafion or directly by electrochemical activation of film electrodes prepared using Pt(IV)–$Cs_{2.5}PW_{12}$. The activation process involves the formation of Pt nanoparticles in situ by cycling the electrode in the potential window 1.1–0 V vs RHE in nitrogen or oxygen atmosphere. Fig. 4 shows some selected cyclic voltammograms recorded during the activation process obtained in a nitrogen saturated 0.5 M H_2SO_4 solution. The numbers on the curves indicate the successive cycles. Curve 1 is almost featureless if one excludes the rapid rise of current near 0 V indicative of hydrogen production. As the number of cycles increases the voltammograms progressively acquire the shape expected for a Pt electrode. The characteristic peaks of hydrogen adsorption/desorption in the potential region 0–0.3 V become progressively more defined together with the Pt/PtO couple in the potential region above O.7 V. This means that the initially present Pt(IV) is progressively reduced to Pt metal forming nanoparticles embedded into or deposited on the insoluble Cs salt. The steady state voltammograms (ca. 30 cycles) is shown in bold. The insert shows two cyclic voltammograms obtained in the same solvent. The one with the two redox couples was obtained with a GC electrode in a 2×10^{-3} M solution of the acid while the dashed curve refers to a film electrode containing Pt free $Cs_{2.5}PW_{12}$ mixed with Vulcan and Nafion in the usual ratio. Over the potential window explored, only one wave is present in the case of the salt. The wave that may be attributed to the first one electron reduction of $Cs_{2.5}H_{0.5}PW_{12}O_{40}$ appears at more negative potentials with respect to the first reduction of the free acid. This is consistent with literature data that predict a negative potential shift of the reduction waves when a less electronegative cations, such as Cs^+, substitute protons in the Keggin structure [65]. The second, and eventually third waves leading to the so-called heteropolyblue structures containing mixed-valent W(VI,V) do not appear in the case of the salt over the potential range explored. The reduction wave of the solid acid partially overlaps the potential region where the characteristic hydrogen adsorption/desorption waves on Pt are present. This leads to errors when one tries to compute the electrochemically active Pt area from the hydrogen adsorption waves.

The electrochemical activation of the catalyst through reduction of Pt(IV) to Pt(0) can also be achieved in oxygen saturated solution. This is clearly demonstrated by the series of RDE voltammograms in Fig. 5a obtained using an electrode similar to the one in Fig. 4 in an oxygen saturated solution. With increasing number of scans a well defined oxygen reduction wave is rapidly developed demonstrating that the Pt reduction actually occurs. For sake of comparison Fig. 5b reports two RDE voltammograms obtained with layers prepared with chemically and electrochemically reduced Pt–$Cs_{2.5}PW_{12}$ with similar Pt loading. As it may be seen the two curves practically overlap thus proving that the two activation methods lead to similar catalytic activity.

In order to demonstrate that the electrochemical activation does not modify the support, X-ray spectra of practical fuel cell electrodes have been taken before and after the activation process in an H_2/O_2 single cell in which the cathodic catalytic layer was prepared with unreduced Pt(IV)–$Cs_{2.5}PW_{12}$. The relative spectra are shown in Fig. 6. As it may be seen, apart from the line broadening probably due to the different components present in the sample, the spectra before and after the activation process are practically the same (see Fig. 1 for comparison) thus demonstrating that the support is not modified by the process leading to reduction of the initially present Pt(IV) to Pt(0).

The response of the electrode and its stability over time has been by further verified in a second experiment by taking successive RDE voltammograms, either using an electrochemically activated

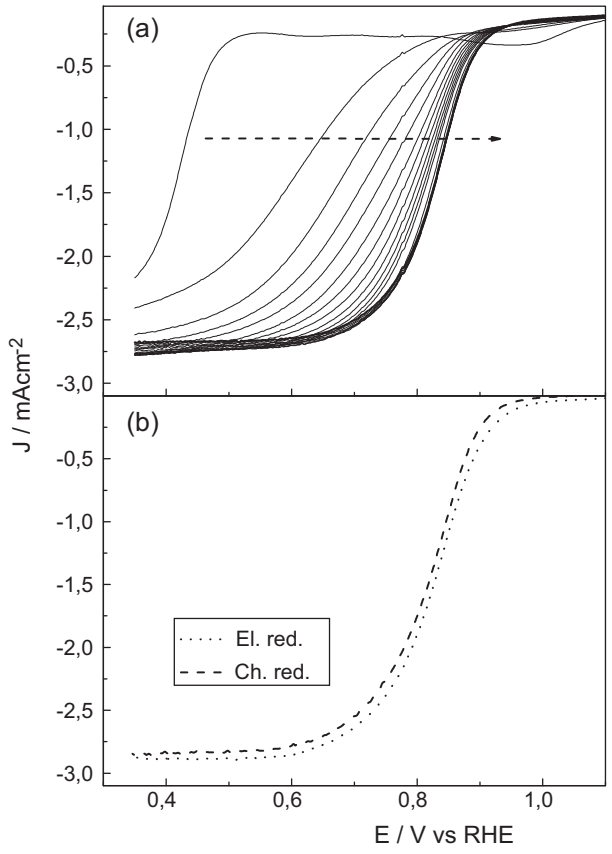

Fig. 5. Series of RDE voltammograms (a) obtained with a Pt–$Cs_{2.5}PW_{12}$ electrode at a scan rate of 5 mV s^{-1} in an oxygen saturated 0.5 M H_2SO_4 solution. Pt loading 30 μg cm^{-2}, 900 rpm. The arrow indicates the increase in the number of polarizations; (b) comparison of RDE voltammograms obtained in oxygen saturated solutions using film electrodes prepared with chemically (- - - -) and electrochemically (···) reduced Pt–$Cs_{2.5}PW_{12}$. Pt loadings ≅16 μg cm^{-2}, 900 rpm, 0.1 M $HClO_4$ solutions.

layer or a film prepared with the chemically reduced composite, in the region of oxygen reduction. Fig. 7 reports some selected curves obtained in an experiment performed using a film electrode prepared with chemically reduced Pt(5%)–$Cs_{2.5}PW_{12}$. Between each RDE voltammogram, the electrode was cycled continuously at

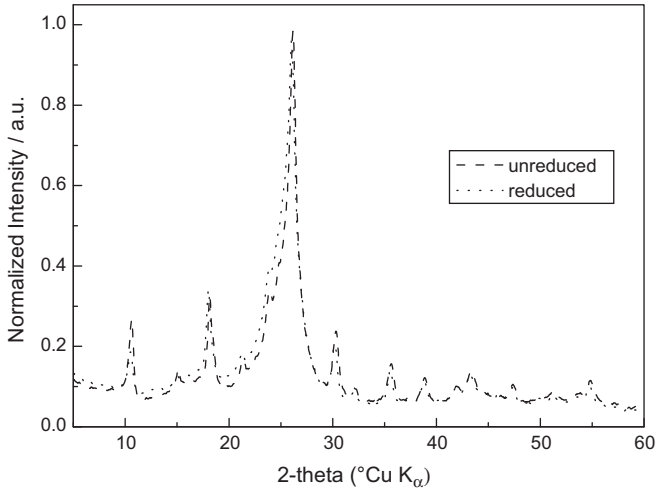

Fig. 6. X-ray spectra of a composite fuel cell electrode containing 5% Pt(IV)–$Cs_{2.5}PW_{12}$ (- - - -) before and (···) and after activation in oxygen. Pt loading 50 μg cm^{-2} (see text for details).

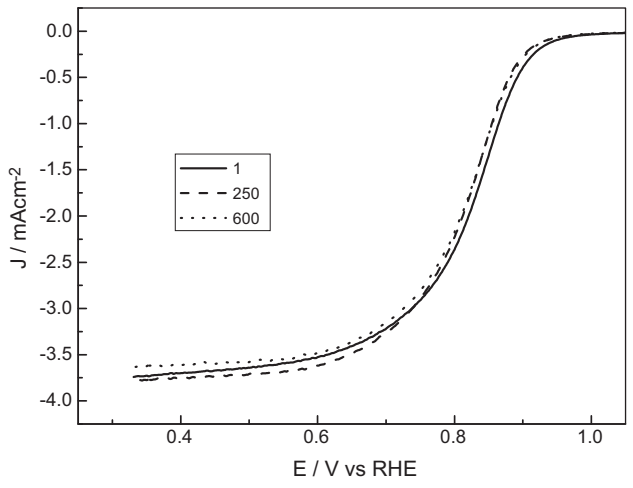

Fig. 7. Series of RDE voltammograms obtained with a Pt(5%)–$Cs_{2.5}PW_{12}$ film electrode, Pt loading 20 μg cm^{-2}, scan rate 5 mV s^{-1}, 900 rpm, 0.5 M H_2SO_4 (see text for details).

50 mV s^{-1} over the potential window 1.1–0 V vs RHE for at least twenty times or until a stable response was obtained. This means that the electrode was cycled more than 12 thousand times over the potential window where Pt undergoes oxidation/reduction processes. The response, as revealed by the overlapping of the RDE voltammograms, demonstrates a rather remarkable stability of the catalytic layer. No systematic decrease of diffusion current, indicative of variations of the electrochemically active surface area (ECSA), or potential shift are observed. The variations are within the limits expected for fluctuations of the experimental conditions (i.e. ambient temperature, atmospheric pressure and/or oxygen saturation). Strictly speaking the ECSA should be determined by measuring the charge associated to the hydrogen adsorption/desorption peaks of the cyclic voltammograms by assuming that the charge associated with a monolayer corresponds to 210 μC cm^{-2} or, alternatively, using the charge associated with CO stripping after controlled CO adsorption (484 μC cm^{-2} for a monolayer). However, none of these methods are applicable in the present case as solid is at least partially electroactive in the region of hydrogen adsorption and, in addition, it is believed to possibly interact with CO [58]. This introduces unknown errors in the measured areas and thus the relevant data will not be quoted.

The previous results clearly demonstrate that well defined and stable oxygen reduction waves can be obtained with electrodes prepared using chemically reduced Pt–$Cs_{2.5}PW_{12}$ or electrodes electrochemically activated. No relevant differences are observed in the responses in spite of the fact that they are structurally different. Having this pointed out, it should be observed that the preparation of the electrode by electrochemical polarization appears to be particularly convenient when a MEA in a real PEMFC is considered [56,57]. This is because the catalytic layer can be activated directly in the cell without a prior chemical reduction step. In addition, electrochemically activated catalytic layers resulted into better behaved electrodes as far as reproducibility the response. This is probably due to the fact that the Pt centers are formed in situ and their morphology/size does not depend on reduction operating conditions such as temperature, hydrogen concentration and time.

3.4. Electrochemical characterization by RRDE

Fig. 8 shows a comparison of RDE voltammograms, positive going sweep, obtained with layers prepared using the reference catalyst 20% Pt on Vulcan XC-72, 5% and 20% Pt–$Cs_{2.5}PW_{12}$

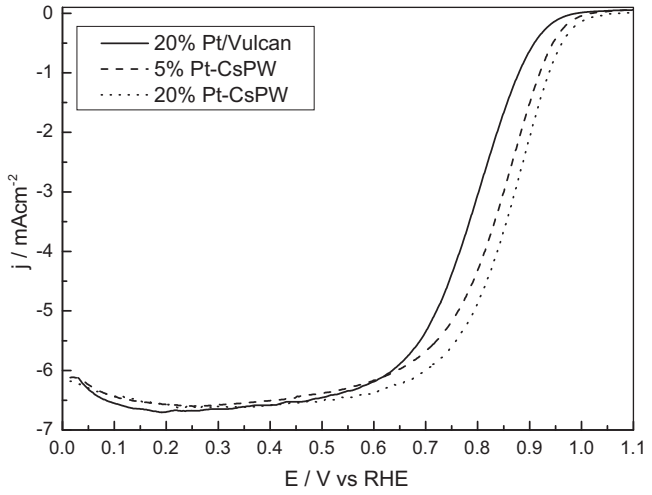

Fig. 8. Comparison of RDE voltammograms obtained at thin film electrodes prepared using (···) 20% Pt–Vulcan (15.8 μg cm^{-2}) (- - - -), Pt(5%)–$Cs_{2.5}PW_{12}$ (16 μg cm^{-2}) Pt(20%)–$Cs_{2.5}PW_{12}$ (17 μg cm^{-2}). Scan rate 5 mV s^{-1}, 2500 rpm rotation rate. Oxygen saturated 0.1 M $HClO_4$ solution.

having comparable Pt loadings (~15–16 μg cm^{-2}). The composite film layer electrodes were activated electrochemically and, after activation, the electrodes were carefully washed with Millipore Milli-Q water and the supporting solution was changed. This procedure was adopted to free the electrode and the solution from chloride ions coming from H_2PtCl_6 that may adsorb on the Pt surface partially poisoning the electrode. The wave pertaining to the composites are displaced in the positive direction when compared with that of the reference catalyst. This testifies that the presence of the insoluble salt improves the catalytic activity of the Pt nanoparticles and is consistent with the results obtained with Pt nanoparticles surface modified using the parent acid [20–23]. The better response, in terms of positive potential shift of the electrode prepared using Pt(20%)–$Cs_{2.5}PW_{12}$ is probably related to the morphology of the composite. At the same Pt loading, an electrode prepared using Pt(20%)–$Cs_{2.5}PW_{12}$ is thinner than one containing Pt(5%)–$Cs_{2.5}PW_{12}$ and, in addition, part of the particles are located at the surface thus facilitating the oxygen access to the catalytic sites. As explained in Section 3.1, the location of the particles, the surface area and the porosity change with the Pt content of the composite salt. This means that several factors such as porosity, surface area, Pt nanoparticle location, in addition to the relative amounts of Nafion and conductive agent, eventually operating in opposition, may affect the overall catalytic activity. To this respect optimization of the electrode performance, also in the case of real fuel cell electrodes requires further attention.

Fig. 9 shows the RDE voltammograms at different rotations speed for 20%Pt/Vulcan XC-72 (Fig. 9a) and for electrochemically activated Pt(5%)–$Cs_{2.5}PW_{12}$ (Fig. 9b) composite electrodes obtained in 0.1 M $HClO_4$ at 25 °C. Similar curves, not shown for sake of simplicity, have been obtained using Pt(20%)–$Cs_{2.5}PW_{12}$. One of the main characteristics of oxygen reduction on Pt is the appearance of hysteresis in the polarization *E*–*j* curve [66]. The oxygen reduction rate is faster in the positive-going potential direction because of the well-known fact that the electrode reaction rate depends on the status of the Pt surface. The hysteresis on the polarization curves may be attributed to the presence of Pt oxide on the negative going direction while the Pt surface is oxide free in the positive scan direction.

Fig. 9c and d shows the molar fractions of H_2O_2 for the two different electrodes computed from the disk and ring currents using the equation ($X_{H_2O_2} = (2I_R/N)/(I_D + I_R/N)$) where I_D and I_R are the disk and ring currents and *N* is the collection efficiency) [66]. The ring potential was set at 1.2 V where the oxidation of H_2O_2 formed at the disc electrode is diffusion limited. The molar fractions of H_2O_2 are only slightly lower for the composite electrode. However, for both layers and for potentials above 0.6 V (i.e. the potential relevant to fuel cell cathodes) H_2O_2 is below 1% indicating that the reduction of O_2 proceeds exclusively via four-electron mechanism.

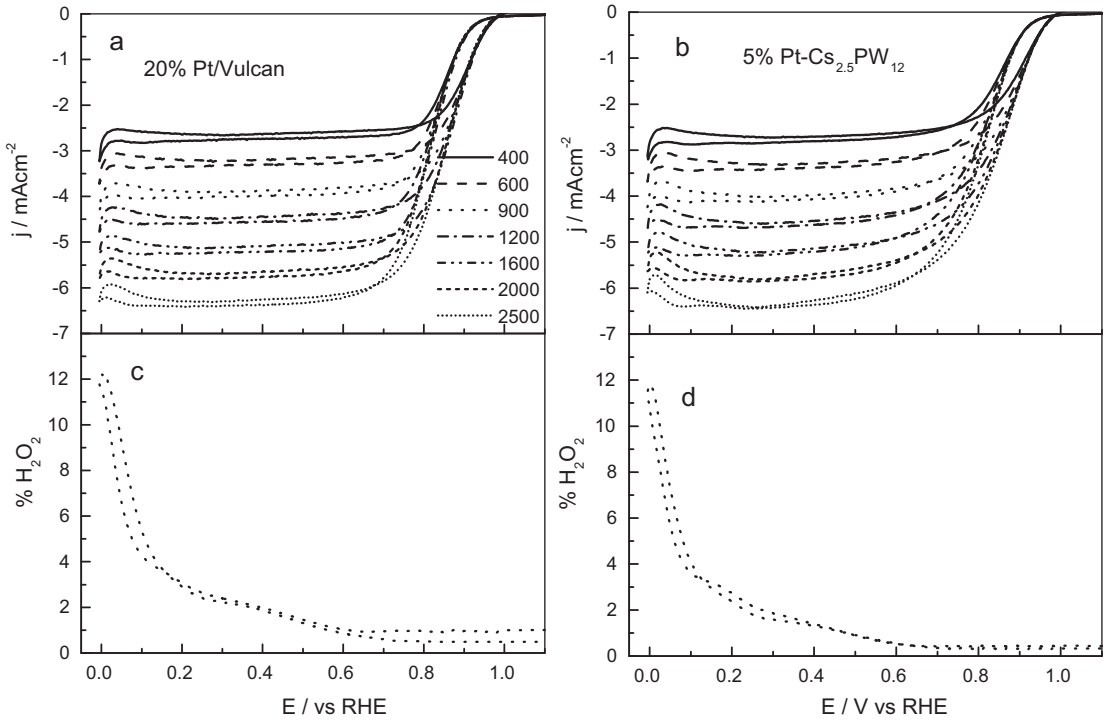

Fig. 9. Forward and reverse RDE voltammograms at different rotation rates obtained with a Pt(5%)–$Cs_{2.5}PW_{12}$ (a) and 20% Pt–Vulcan (b) film electrodes in 0.1 M $HClO_4$ solution saturated with oxygen. Pt loadings at 16 and 15.8 μg cm^{-2}, respectively. (c) and (d) Ring currents measured at 1.2 V vs RHE and 1600 rpm.

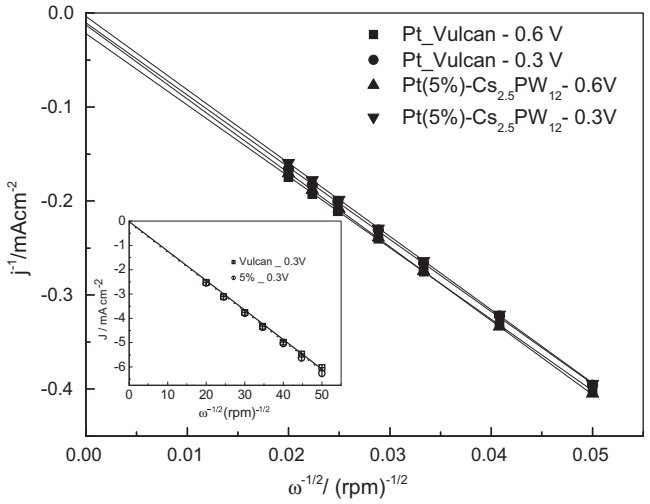

Fig. 10. Koutechy–Levich reciprocal plot obtained using the data in Fig. 8. The insert shows the Levich dependence of the current densities on the square root of the rotation rate.

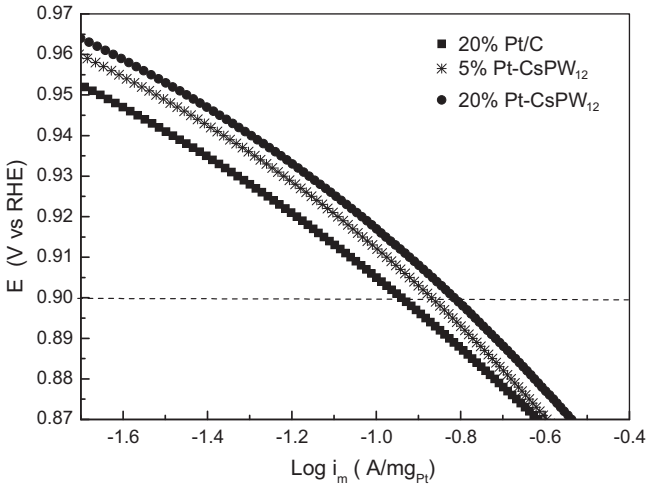

Fig. 11. Typical low overpotential region Tafel plots from the positive going branches of RDE voltammograms obtained with film electrodes containing (●) Pt(20%)–$Cs_{2.5}PW_{12}$, (*) Pt(5%)–$Cs_{2.5}PW_{12}$ and (■) 20% Pt–Vulcan. Rotation rate 2500 rpm, potential scan rate 5 mV s^{-1}. Oxygen saturated O.1 M $HClO_4$ solution.

H_2O_2 formation becomes evident at potentials negative of 0.6 V and increase significantly in the H_{upd} region. This is also evident from the decrease of the disk current density at very low potentials. No relevant differences between the positive and negative going potential scan is observed.

RDE voltammetric limiting current densities (j_{lim}) can be expressed as follows [22]:

$$j_{lim}^{-1} = (nFkC_{film}C_{Ox})^{-1} + j_L^{-1} \quad (1)$$

where j_L is given by the Levich equation in which the convective diffusion component is proportional to the square root of the rotation rate, k is the rate constant for the catalytic reaction in homogeneous units, C_{film} is the surface concentration of the catalyst and C_{Ox} is the oxygen bulk concentration. The other symbols F and n stand for the Faraday constant and number of electrons involved in the electrochemical reaction ($n = 4$ for the present case). Eq. (1) is equivalent to the well known Koutecky–Levich equation in which the term relative to the charge propagation (electrons and protons) within the catalytic layer are expected to be fast and thus the oxygen reactant has easy access to the dispersed active sites. Because of the low amount of Nafion added to the ink and of the high porosity of the Cs salt, the effect of the thickness of the layer on the measured current densities can be considered as relatively negligible. In other words, this is equivalent to assume that the transport of oxygen from the solution to the catalytic sites is unaffected by the presence of the film. The KL reciprocal plots for the two electrodes, constructed using the data taken from the positive going scans at the two different potentials 0.3 V and 0.6 V, are shown in Fig. 10. The insert shows the corresponding Levich plots. The KL plots for both electrodes are linear with a non-zero intercept as expected for a kinetically limited process. The linearity also indicates that the kinetic limitations are not originated from slow charge propagation or slow diffusion of oxygen through the catalytic film that would result into non-linearity [67]. Hence, non-zero intercepts can be assumed as proportional to the rate constant for the catalytic reaction.

The estimated values of kC_{film}, that are equivalent to the intrinsic rates of heterogeneous charge transfer, are ca. 6. 6×10^{-1} and 2.2×10^{-1} cm s^{-1} at 0.3 V for the composite electrode and the reference 20% Pt/C, respectively. The corresponding values computed at 0.6 V are ca. 2.4×10^{-1} cm s^{-1} and 1.1×10^{-1} cm s^{-1}, respectively, reflecting a probable decrease of k at less negative potential. All these results are reproducible within 10%. Quite similar results, omitted for sake of brevity, have been obtained using Pt(20%)–$Cs_{2.5}PW_{12}$ or with catalytic layers prepared using the chemically or electrochemically reduced composites.

The results demonstrate that supporting the Pt nanoparticles on the insoluble acid salt enhances (ca. 2–3 times) the intrinsic rate of heterogeneous charge transfer thus confirming the results obtained in the case of the incorporation of the free heteropolytungstate acid into inks of Pt nanoparticles or Vulcan supported Pt [20–23].

The reciprocals of the slopes of the KL plots are equivalent to the term BC_{0x} of the Levich equation for rotating disk voltammetry. The computed average values in the potential range 0.3–0.7 V for the two electrodes are close to $13.4 \pm 0.6 \times 10^{-2}$ cm^{-2} $rpm^{-0.5}$ vs a theoretical value of 14.28×10^{-2} cm^{-2} $rpm^{-0.5}$ calculated assuming $n = 4$, an O_2-solubility of 1.18 mol m^{-3} and O_2-diffusivity of 1.9×10^{-9} m^2 s^{-1} and a water viscosity equal to 0.893×10^{-2} cm^2 s^{-1} [68]. Given the uncertainties of the literature data on the oxygen solubility and diffusivity and together with the evidences obtained for H_2O_2 production by the ring data, the results demonstrate that the oxygen reduction involves four electrons.

The catalytic properties of fuel cell catalyst may also be estimated [61] in terms of mass (A mg_{Pt}^{-1}) or specific activities (A cm_{Pt}^{-2}). The relevant values may be deduced from Tafel type plots E vs log i_m (where i_m is the mass transfer corrected kinetic current $((j_{lim}j)/(j_{lim} - j))$ divided by the mass of platinum) measured at 0.9 V vs RHE where the influence of mass transport is negligible. The Tafel plots obtained from the experimental curves in Fig. 9 have slopes that are changing continuously from −2.3 RT/F at low overpotentials ($E > 0.85$) to -2×2.3 RT/F at high overpotentials ($E < 0.85$). This is rather usual in the case of oxygen reduction [61]. Fig. 11 shows the Tafel plots for different types of electrodes in the low potential region. The slopes are close to −70 mV per decade consistent with an oxygen reduction mechanism involving a Temkin type isotherm. The computed values of the mass specific activities at 0.9 V are 0.114, 0.135 and 0.153 A mg_{Pt}^{-1} for 20% Pt–Vulcan, 5% and 20% Pt–$Cs_{2.5}PW_{12}$ electrodes, respectively, as expected from the previous data. The value of the unmodified electrode is comparable with that listed in Ref. [61] (0.13 A mg_{Pt}^{-1}) obtained at 60 °C. For the reasons given in discussing the cyclic voltammetric data, it was impossible to derive the corresponding values of the specific activity as the electrochemical active area has proven to be difficult to measure.

An additional evidence of the efficiency of the catalyst also at low Pt content has been obtained by assembling a fuel cell in which

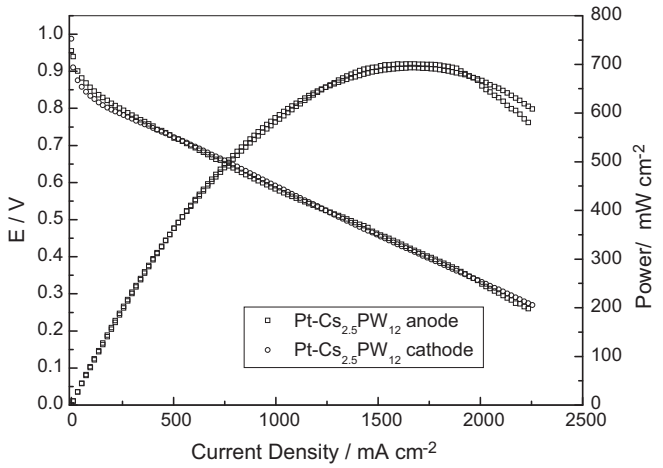

Fig. 12. Polarization curves obtained with a MEA assembled using an E-TEK Gas Diffusion Electrode, Pt loading 0.5 mg cm^{-2}, and Pt(IV)–$Cs_{2.5}PW_{12}$ (Pt(IV) loading: 0.2 mg cm^{-2}) on Toray paper. Membrane Nafion 212; cell temperature: 70 °C, feed gas H_2 100 cm^3 min^{-1}, O_2 200 cm^3 min^{-1}, 100% humidification, 2 bar.

one electrode was a commercial Gas Diffusion Electrode (GDE) from E-TEK (Pt loading: 0.5 mg cm^{-2}) and the other was prepared using Pt(IV)–$Cs_{2.5}PW_{12}$ (Pt loading: 0.2 mg cm^{-2}). The activation was achieved by feeding humidified hydrogen and oxygen to the commercial (anode) and to the Pt(IV)–$Cs_{2.5}PW_{12}$ based (cathode) electrode, respectively. The cathode potential was brought in step down to 0.2 V to achieve complete Pt(IV) reduction to Pt(0). At the end of the process, that takes 2–3 h, the OCV of the cell reached a value close to 0.96 V, signifying complete Pt reduction. The two polarization curves and the relative power curves in Fig. 12 have been obtained by using the Pt–$Cs_{2.5}PW_{12}$ based electrode as anode or as cathode by switching the feed gases. Before changing from one feed gas to the other the cell was purged with argon for 10–5 min. As it may be seen the responses are practically the same. This means that Pt loadings of the order of 200 μg cm^{-2} with nanoparticles embedded into the porous structure of the insoluble Cs salt are largely sufficient to realize an efficient catalyst for oxygen reduction and that the composite catalyst works well also for hydrogen oxidation. Details on this procedure and on the realization of low Pt content fuel cells using Pt–$Cs_{2.5}PW_{12}$ at both electrodes will be the subject of a further paper.

Two likely hypotheses may be put forward to explain the reasons of the improvement of the catalytic activity of the Pt nanoparticles supported by the insoluble mesoporous $Cs_{2.5}H_{0.5}PW_{12}O_{40}$ solid acid with respect to the standard catalyst. First of all, due to the peculiar structure of the salt, the Pt nanoparticles trapped in the pores cannot grow above certain dimensions. This is the same concept exploited in organic catalysis where this type of salt are used as shape selective catalyst by regulating the dimensions of the pores to accommodate a particular reactants. The inclusion of the metallic particles in the pores of $Cs_{2.5}PW_{12}$ causes a decrease of the surface area and hence of the permeability of the gases. However, sufficient voids remain also in the case of the higher Pt content. This does not limit the transport properties of the catalytic layer [56,57]. Being mostly trapped the particles are less prone to be subject to aggregation phenomena. This is proved by the high stability of the response of the electrode under repeated polarization in the oxygen reduction region (see Fig. 6). The same stability under real fuel cell conditions has already been proved [56,57].

The second reason may be related to the high surface acidity of the salt. The Pt nanoparticles are located in an environment very rich of high mobile protons that are necessary to support the four-electron reduction of oxygen to water. This makes the composite catalyst very promising for the preparation of fuel cell electrodes very effective also at low Pt loading for both oxygen reduction and hydrogen oxidation.

4. Conclusion

The results obtained demonstrate that supporting Pt nanoparticles on zeolitic-type mesoporous $Cs_{2.5}H_{0.5}PW_{12}O_{40}$ solid superacid results in the enhancement of the electrocatalytic reduction of oxygen in terms of two–threefold increase of the heterogeneous rate constant and in a positive shift of the electroreduction potential. Stable catalytic layers containing Pt–$Cs_{2.5}PW_{12}$ can be easily prepared by mixing chemically reduced Pt(IV)–$Cs_{2.5}PW_{12}$ with carbon and Nafion or by direct electrochemical activation. The layers contain Pt nanoparticles embedded into the pores of the solid acid and the enhanced catalytic activity has probably to be ascribed to the high surface acidity of the salt and high proton mobility that support the four-electron reduction of oxygen to water.

Acknowledgements

This research has been carried out within the NUME Project "Development of composite proton membranes and of innovative electrode configurations for polymer electrolyte fuel cells"(MIUR, FISR 2003).

Partial support for A. Kolary by Ministry of Science and Higher Education (Poland) under research projects N204164324284, 70/N-SINGAPUR/2007/0, and N507/8226 (doctoral, awarded to A.K.-Z.) is also acknowledged.

We thank Eric Larquet, Agnieszka Witkowska, Marco Minicucci for HRTEM investigations, Prof. Marina Mastragostino, F. Soave (University of Bologna) for the BET measurements and Prof. Gabriele Giuli for X-ray measurements.

References

[1] F.A. deBruijn, V.A.T. Dam, G.J.M. Janssen, Fuel Cell 8 (2008) 3.
[2] R. Borup, J. Meyers, B. Pivovar, Y. Seung Kim, R. Mukundan, N. Garland, D. Myers, M. Wilson, F. Garzon, D. Wood, P. Zelenay, K. More, K. Stroh, T. Zawodinski, J. Boncella, J.E. McGrath, M. Inaba, K. Miyatake, M. Hori, K. Ota, Z. Ogumi, S. Miyata, A. Nishikata, Z. Sirona, Y. Uchimoto, K. Yasuda, K. Kimijima, N. Iwashita, Chem. Rev. 107 (2007) 3904.
[3] X. Xu, S. Xe, J. Power Sources 172 (2007) 145.
[4] M. Nose, T. Kinumoto, H.S. Choo, K. Miyazaki, T. Abe, Z. Ogumi, Fuel Cell 9 (2009) 284.
[5] L.M. Roen, C.H. Paik, T.D. Jarvi, Electrochem. Solid State Lett. 7 (2004) A19.
[6] D.A. Stevens, M.T. Hicks, G.M. Haugen, J.R. Dahn, J. Electrochem. Soc. 152 (2005) A2309.
[7] M. Cai, M.S. Ruthkosky, B. Merzougui, S. Swathirajan, M.P. Balog, S.E. Oh, J. Power Sources 160 (2006) 977.
[8] H. Ekström, B. Wickman, M. Gustavsson, P. Hanarp, L. Eurenius, E. Olsson, G. Lindbergh, Electrochim. Acta 52 (2007) 4239.
[9] S. von Kraemer, K. Wikander, G. Lindbergh, A. Lundblad, A.E.C. Palmqvist, J. Power Sources 108 (2008) 185.
[10] T. Ioroi, Z. Siroma, N. Fujiwara, S. Yamazaki, K. Yasuda, Electrochem. Commun. 7 (2005) 183.
[11] J. Shim, C.R. Lee, H.K. Lee, J.S. Lee, E.J. Cains, J. Power Sources 102 (2001) 172.
[12] S.Y. Huang, P. Ganesan, S. Park, B.N. Popov, J. Am. Chem. Soc. 131 (2009) 13898.
[13] S. Shanmungam, A. Gedanken, J. Phys. Chem. C 113 (2009) 18707.
[14] H. China, S. Campbell, O. Kesler, J. Electrochem. Soc. 156 (2009) B1232.
[15] X. Liu, J. Chen, G. Liu, L. Zhang, H. Zhang, B. Yi, J. Power Sources 195 (2010) 4098.
[16] P.J. Kulesza, L.R. Faulkner, J. Electroanal. Chem. 259 (1989) 81.
[17] P.J. Kulesza, B. Grzybowska, M.A. Malik, M.T. Galkowski, J. Electrochem. Soc. 144 (1997) 1991.
[18] D.P.J. Kulesza, L.R. Faulkner, J. Electrochem. Soc. 136 (1989) 707.
[19] P.J. Kulesza, M. Chojak, K. Karnicka, K. Miecznikowski, B. Palys, A. Lewera, Chem. Mater. 16 (2004) 4128.
[20] R. Wlodarczyk, M. Chojak, K. Miecznikowski, A. Kolary, P.J. Kulesza, R. Marassi, J. Power Sources 159 (2006) 802.
[21] P.J. Kulesza, K. Karnicka, K. Miecznikowski, M. Chojak, A. Kolary, P.J. Barczuk, G. Tsirlina, W. Czerwinski, Electrochim. Acta 50 (2005) 5155.
[22] R. Wlodarczyk, A. Kolary-Zurowska, R. Marassi, M. Chojak, P.J. Kulesza, Electrochim. Acta 52 (2007) 3958.

[23] M. Chojak, A. Kolary-Zurowska, R. Wlodarczyk, K. Miecznikowski, K. Karnicka, B. Palys, R. Marassi, P.J. Kulesza, Electrochim. Acta 52 (2007) 5574.
[24] R.J. Stanis, M.C. Kuo, A.J. Rickett, J.A. Turner, A.M. Herring, Electrochim. Acta 53 (2008) 8277.
[25] Z. Cui, W. Xing, C. Liu, D. Tian, H. Zhang, J. Power Sources 195 (2010) 1619.
[26] P. Pan, J. Chen, W. Tao, L. Nie, S. Yao, Langmuir 22 (2006) 5872.
[27] M.H. Seo, S.M. Choi, H.J. Kim, B.K. Cho, W.B. Kim, J. Power Sources 179 (2008) 81.
[28] M. Chojak, M. Mascetti, R. Wlodarczyk, R. Marassi, K. Karnicka, K. Miecznikowski, P.J. Kulesza, J. Solid State Electrochem. 8 (2004) 854.
[29] B.R. Limoges, R.J. Stanis, J.A. Turner, A.M. Herring, Electrochim. Acta 50 (2005) 1169.
[30] M.C. Kuo, R.J. Stanis, J.R. Ferrell III, J.A. Turner, A.M. Herring, Electrochim. Acta 52 (2007) 2051.
[31] J.R. Ferrell III, M-C. Kuo, J.A. Turner, A.M. Herring, Electrochim. Acta 53 (2008) 4927.
[32] R.J. Stanis, M-C. Kuo, J.A. Turner, A.M. Herring, J. Electrochem. Soc. 155 (2008) B155.
[33] J.R. Ferrel III, M.-C. Kuo, A.M. Herring, J. Power Sources 195 (2010) 39.
[34] Y.S. Kim, F. Wang, M. Hickner, T.A. Zawodzinski, J.E. McGrath, J. Membr. Sci. 212 (2003) 263.
[35] V. Ramani, H.R. Kunz, J.M. Fenton, J. Membr. Sci. 232 (2004) 31.
[36] V. Ramani, H.R. Kunz, J.M. Fenton, J. Membr. Sci. 266 (2005) 110.
[37] V. Ramani, H.R. Kunz, J.M. Fenton, J. Power Sources 152 (2005) 182.
[38] V. Ramani, H.R. Kunz, J.M. Fenton, Electrochim. Acta 50 (2005) 1181.
[39] V. Ramani, H.R. Kunz, J.M. Fenton, J. Membr. Sci. 279 (2006) 506.
[40] M. Li, Z.G. Shao, H. Zhang, Y. Zhang, X. Zhu, B. Yi, Electrochem. Solid State Lett. 9 (2006) A92–A95.
[41] Y. Zhang, H. Zhang, C. Bi, X. Zhu, Electrochim. Acta 53 (2008) 4096–4103.
[42] M. Amirinejad, S.S. Madaeni, M.A. Navarra, E. Rafiee, B. Scrosati, J. Power Sources 196 (2011) 988.
[43] Y. Izumi, M. Ogawa, K. Urabe, Appl. Catal. A: Gen. 132 (1995) 127.
[44] S. Soled, S. Miseo, G. Mc Vicker, W.E. Gates, A. Gutierrez, J. Paes, Catal. Today 36 (1997) 441.
[45] G. Koyano, K. Ueno, M. Misono, Appl. Catal. A: Gen. 181 (1999) 267.
[46] T. Okuhara, H. Watanabe, T. Nishimura, K. Inumaru, M. Misono, Chem. Mater. 12 (2000) 2230.
[47] Z. Zhu, W. Yang, J. Phys. Chem. C 113 (2009) 17025.
[48] L.R. Pizzio, M.N. Blanco, Appl. Catal. A: Gen. 255 (2003) 265.
[49] T. Okuhara, T. Nakato, Catal. Surv. Jpn. 2 (1998) 31.
[50] T. Okuhara, Chem. Rev. 102 (2002) 3641.
[51] T. Kukino, R. Kikuchi, T. Takeguki, T. Matsui, K. Eguchi, Solid State Ionics 176 (2005) 1845.
[52] T. Okuhara, Appl. Catal. A: Gen. 256 (2003) 213.
[53] Y. Liu, K. Na, M. Misono, J. Mol. Catal. A 141 (1999) 145–153.
[54] Y. Yoshinaga, T. Suzuki, M. Yoshimune, T. Okuhara, Top. Catal. 19 (2002) 179.
[55] A. Abdullah, E.F. Kozhevnikova, I.V. Kozhevnikov, Appl. Catal. A: Gen. 378 (2010) 11.
[56] B. Scrosati, R. Marassi, A., Kolari, A., Zurowsky, P.J. Kulesza, S. Dsoke, Catalizzatori a basso contenuto in Pt per celle a combustible, Italian Patent No. RM2007A000228 (2007).
[57] B. Scrosati, R. Marassi, A., Kolari, A. Zurowsky, P.J. Kulesza, S. Dsoke, Catalyst having low Pt content for fuel cells, PTC/IB2008/051462 (2008).
[58] A. Zurowky, A. Kolary-Zurowska, S. Dsoke, P.J. Barzuk, R. Marassi, P.J. Kulesza, J. Electroanal. Chem. 649 (2010) 238.
[59] S. Dsoke, A. Moretti, G. Giuli, R. Marassi, Int. J. Hydrogen Energy 36 (2011) 8098.
[60] A. Kolary-Zurowska, A. Zurowski, R. Marassi, P.J. Kulesza, ECS Trans. 33 (2010) 131.
[61] H.A. Gasteiger, S.S. Kocha, B. Sompalli, F.T. Wagner, Appl. Catal. B: Environ. 56 (2005) 9.
[62] G.M. Brown, M.R. Noe-Spirletr, W.R. Busing, H.A. Levy, Acta Crystallogr. B 33 (1977) 1038.
[63] M. Yoshimune, Y. Yoshinaga, T. Okuhara, Microporous Mesoporous Mater. 51 (2002) 165.
[64] E. Principi, A. Witkowska, S. Dsoke, R. Marassi, A. DiCicco, Phys. Chem. Chem. Phys. 11 (2009) 9987.
[65] M. Ai, Appl. Catal. 4 (1982) 245.
[66] U.A. Paulus, T.J. Schmidt, H.A. Gasteiger, R.J. Behm, J. Electroanal. Chem. 495 (2001) 134.
[67] C.P. Andrieux, J.M. Dumas-Bouchiat, J.M. Saveant, J. Electroanal. Chem. 131 (1982) 1.
[68] U.A. Paulus, V. Stamenkovic, V. Radmilovic, N.M. Markovic, P.N. Ross, J. Phys. Chem. B 106 (2002) 4181.